Journal of Materials Chemistry A

COMMUNICATION

View Article Online
View Journal | View Issue

Cite this: J. Mater. Chem. A, 2018, 6, 17861

Received 14th July 2018
Accepted 28th August 2018

DOI: 10.1039/c8ta06804f

rsc.li/materials-a

Post-synthetic modification of metal–organic frameworks for chiral gas chromatography†

Wen-Ting Kou, [a] Cheng-Xiong Yang *[a] and Xiu-Ping Yan *[b]

Chiral metal–organic frameworks (MOFs) show great potential in chiral catalysis and separation. However, their application is still hindered by the limited availability of chiral MOFs and chiral recognition centers due to the great challenges for direct synthesis of chiral MOFs with designed chiral recognition sites. Here we report a post-synthesis approach for the facile preparation of chiral MOFs for chiral gas chromatography. Five chiral MOFs with an identical parent framework but different chiral recognition sites were synthesized *via* grafting various chiral recognition sites of ligands onto MIL-101–NH_2. The chiral MOF-coated capillary columns gave good resolution for the separation of diverse racemates with superior separation to the commercial chiral capillary columns. The results reveal that the post-synthesis approach is convenient to fabricate target chiral MOFs with pre-designed functions with the ability to avoid blind synthesis of chiral MOFs *via* direct synthesis and to facilitate the evolution of chiral stationary phases in chiral chromatography.

Chirality is an essential property of nature and plays significant roles in pharmacology, agrochemicals, biology, chemistry and many other areas.[1] Separation of chiral enantiomers into two pure individual enantiomers is of great significance as two pure enantiomers may differ in biological activity, pharmacology and toxicity in many cases.[2] Chiral separation is challenging due to the same physical or chemical properties of chiral enantiomers. Considering the importance and challenge of chiral separation, plenty of chiral recognition materials and techniques have been explored.[1–7] Chromatography relying on chiral stationary phases (CSPs) has been proved to be the most applicable approach in chiral separation.[3,4] Columns packed or coated with CSPs are the core of chiral chromatography. Thus, it is crucial to develop novel CSPs for chiral chromatography.

Recently, porous materials such as porous organic cages, covalent organic frameworks, metal–organic frameworks (MOFs) and porous organic frameworks have been explored as advanced CSPs for chiral chromatography.[5–7] In particular, chiral MOFs have received great attention due to their good spatial selectivity for three dimensional frameworks built from inorganic metal clusters and organic linkers. Their diversity in structure and pore size, high surface area and selective adsorption affinity make chiral MOFs attractive as chiral separation media.[8–13] The special microporosity of chiral MOFs and unique MOF structures provide a befitting environment for enantioseparation. Up to now, chiral MOFs constructed with chiral organic linkers have been applied in chiral chromatography with good resolution and selectivity.[14–17]

General strategies to synthesize chiral MOFs can be summarized as direct synthesis and post-synthesis. Rational design of chiral MOFs is usually difficult for the direct synthesis as many uncontrollable factors may hinder the synthesis of designed chiral MOFs. Moreover, the synthesis of chiral MOFs often requires complex and costly chiral starting materials. Post-synthetic modification (PSM) is an attractive method to obtain sophisticated functional materials due to economic and convenient synthetic processes and the available varieties of functionalized organic groups.[18,19] PSM allows designed chiral functional groups to be controllably introduced into MOFs.[20–25] Although the introduction of designed chiral recognition sites to control chiral selectivity is of great significance for chiral separation, the PSM process to synthesize designed chiral MOFs for chiral chromatography has never been reported so far.

Herein, we report a PSM strategy to synthesize chiral MOFs with designed chiral recognition sites for chiral gas chromatography (GC) separation of diverse racemates. An amino-containing MOF MIL-101(Al)–NH_2 was chosen as the parent MOF because of its large surface area, and good thermal and

[a]College of Chemistry, Research Center for Analytical Science, Tianjin Key Laboratory of Molecular Recognition and Biosensing, Nankai University, Tianjin 300071, China. E-mail: cxyang@nankai.edu.cn

[b]State Key Laboratory of Food Science and Technology, International Joint Laboratory on Food Safety, Institute of Analytical Food Safety, School of Food Science and Technology, Jiangnan University, Wuxi 214122, China. E-mail: xpyan@jiangnan.edu.cn

† Electronic supplementary information (ESI) available. See DOI: 10.1039/c8ta06804f

chemical stability.[26] In addition, the high activity of the amino group on the framework to carboxylic acid, isocyanates, anhydrides and alkenes[27–31] is quite favorable for PSM. The large pore windows and pores of MIL-101(Al)–NH_2 (ref. 26) also allow the designed molecules to get in. Five chiral molecules with different chiral recognition sites were, respectively, grafted onto MIL-101(Al)–NH_2 *via* covalent bonds to obtain five chiral MOFs MIL-101(Al)–Xs (Xs represents the specific chiral organic groups) with good stability and different chiral selectivities (Fig. 1). Chiral MOF-coated capillary columns were also fabricated for the chiral GC separation of diverse racemates. The resolution of some of these racemates on these chiral capillary columns was superior to that of the commercial chiral capillary columns. The results reveal the promising aspects of the chiral modification of MOFs *via* PSM and the great potential of chiral post-modified MOFs as novel CSPs for chiral separation.

Chiral groups or chiral centers in MOFs play significant roles in chiral separation and catalysis.[32] In addition, chiral selectivity and the chiral separation mechanism are also closely related to chiral groups or chiral centers. Therefore, we selected five chiral molecules with different chiral groups or chiral centers to construct five chiral MOFs with the same MOF framework but various chiral groups or chiral centers to elucidate the effect of chiral group or chiral center on chiral separation. (*S*)-2-Phenylpropionic acid, (*R*)-1,2-epoxyethylbenzene, (+)-diacetyl-L-tartaric anhydride, L-proline, and (1*S*)-(+)-10-camphorsulfonyl chloride were employed as the post-synthetic molecules (Fig. 1). (*S*)-2-Phenylpropionic acid and (*R*)-1,2-epoxyethylbenzene represent chiral aromatic amide and aromatic epoxy, respectively, providing the possibility for π–π and hydrogen-bonding interactions with analytes during chiral separation. However, their hydrogen-bonding sites are quite different. (+)-Diacetyl-L-tartaric anhydride represents chiral anhydride, offering hydrogen-bonding interactions with chiral analytes. L-Proline represents chiral amino acid, in which the nitrogen provides hydrogen-bonding interactions with the analytes. (1*S*)-(+)-10-Camphorsulfonyl chloride represents chiral acyl chloride, in which the alkyl provides weak chiral interactions with the analytes. Therefore, we try to use the above five types of chiral molecule-modified MIL-101(Al)–Xs to explore the effect of the post-modified chiral group on chiral separation.

All the chiral MOFs were obtained *via* the covalent bonding between the amine groups on MIL-101(Al)–NH_2 and the chiral precursors. Fourier transform-infrared (FT-IR) and circular dichroism (CD) spectroscopy, ^{1}H nuclear magnetic resonance (NMR) analysis, X-ray diffraction (XRD), thermogravimetric analysis (TGA), N_2 adsorption–desorption, and scanning electron microscopy (SEM) experiments were performed to characterize the synthesized MIL-101(Al)–NH_2 and chiral MIL-101(Al)–Xs (Fig. 2 and 3). The existence of the characteristic bands of MIL-101(Al)–NH_2 (red) in the FT-IR spectra of MIL-101(Al)–Xs (black) reveals that the parent MOF is intact and stable during the PSM (Fig. 2). In addition, the appearance of the characteristic bands of amide groups at approximately 1670 cm^{-1} (C–N) and the characteristic bands of chiral groups (blue) indicates the successful chemical grafting of the chiral groups on MIL-101(Al)–Xs (Fig. 2a–e). For MIL-101–*S*-2-Ppa, the band at 1675 cm^{-1} is the characteristic band of the amide N–C=O stretching vibration, while the bands at 1604 and 854 cm^{-1} are the characteristic bands of (*S*)-2-phenylpropionic acid (Fig. 2a). The bands at 978 (C–O stretching vibration) and 693 cm^{-1} in MIL-101–*R*-Epo are the characteristic bands of (*R*)-1,2-epoxyethylbenzene (Fig. 2b). The bands in MIL-101–(+)-Ac-L-Ta at 1746, 1223 and 1076 cm^{-1} are ascribed to the C=O and C–O stretching vibrations, and all these bands correspond to the characteristic bands of (+)-diacetyl-L-tartaric anhydride (Fig. 3c). The bands at 1604 and 1085 cm^{-1} in MIL-101–L-Pro are attributed to the C–N stretching vibration and out-of-plane bending vibration of L-proline, respectively (Fig. 2d). The band at

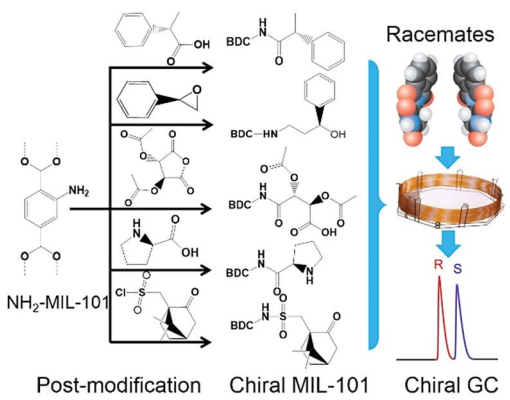

Fig. 1 Schematic illustration of the post-synthesis of chiral MIL-101(Al)–Xs and the fabrication of their coated capillary columns for chiral GC.

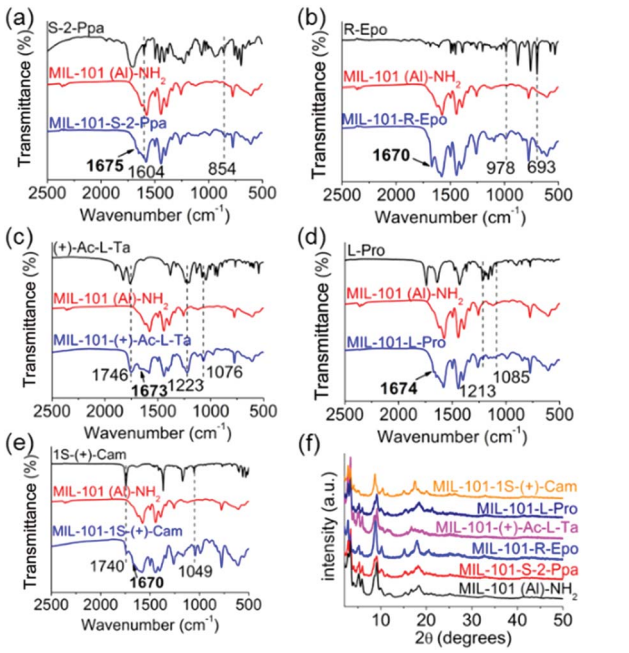

Fig. 2 FT-IR spectra (a–e) and XRD patterns (f) of MIL-101(Al)–NH_2 and MIL-101(Al)–Xs. *S*-2-Ppa, *R*-Epo, (+)-Ac-L-Ta, L-Pro and 1*S*-(+)-Cam refer to (*S*)-2-phenylpropionic acid, (*R*)-1,2-epoxyethylbenzene, (+)-diacetyl-L-tartaric anhydride, L-proline, and (1*S*)-(+)-10-camphorsulfonyl chloride, respectively.

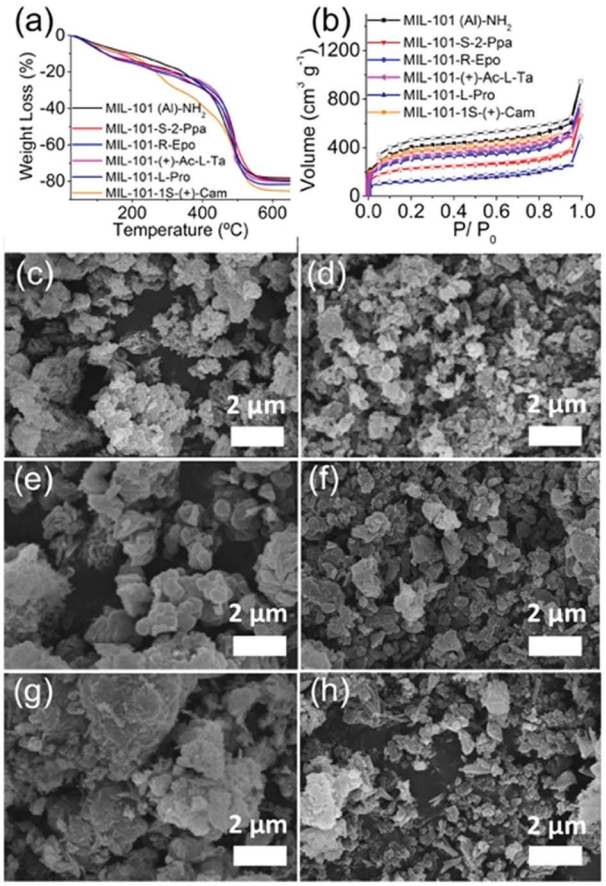

Fig. 3 (a) TGA curves and (b) N_2 adsorption–desorption isotherms of MIL-101(Al)–NH_2 and MIL-101(Al)–Xs. SEM images of (c) MIL-101(Al)–NH_2, (d) MIL-101–*S*-2-Ppa, (e) MIL-101–*R*-Epo, (f) MIL-101–(+)-Ac-L-Ta, (g) MIL-101–L-Pro, and (h) MIL-101–1*S*-(+)-Cam.

1740 cm^{-1} in MIL-101–1*S*-(+)-Cam is attributed to the C=O stretching vibration of ketone, while the band at 1049 cm^{-1} is attributed to the S=O asymmetric stretching vibration, and all these bands correspond to the characteristic bands of (1*S*)-(+)-10-camphorsulfonyl chloride. ^1H NMR analysis shows that about 29%, 19%, 33%, 15% and 4.7% chiral Xs were grafted onto MIL-101(Al) for obtaining MIL-101–*S*-2-Ppa, MIL-101–*R*-Epo, MIL-101–(+)-Ac-L-Ta, MIL-101–L-Pro and MIL-101–1*S*-(+)-Cam, respectively (Fig. S1, ESI†).

The CD spectra were further studied to characterize the chiral MIL-101(Al)–Xs (Fig. S2, ESI†). The CD spectra of MIL-101–*R*-Epo, MIL-101–L-Pro, MIL-101–1*S*-(+)-Cam and MIL-101–*S*-2-Ppa exhibit typical single curves, which prove the homochirality of these chiral MOFs. The extremely weak CD intensity of MIL-101–(+)-Ac-L-Ta was caused by the weak ultraviolet absorption of (+)-Ac-L-Ta.

The XRD patterns of the MIL-101(Al)–Xs (Fig. 2f) are in good agreement with that of the synthesized MIL-101(Al)–NH_2 (black), showing that the grafting of chiral groups *via* PSM had no obvious effect on the crystallinity of MIL-101(Al)–NH_2. No obvious weight loss for all MIL-101(Al)–Xs compared with MIL-101(Al)–NH_2 shows the good thermal stability of MIL-101(Al)–Xs (Fig. 3a). The Brunauer–Emmett–Teller (BET) surface area (Fig. 3b) of MIL-101(Al)–NH_2 is 1292 $m^2\ g^{-1}$, while the BET surface areas of MIL-101(Al)–Xs decrease to 1276, 441, 819, 1080 and 1162 $m^2\ g^{-1}$ for MIL-101–*S*-2-Ppa, MIL-101–*R*-Epo, MIL-101–(+)-Ac-L-Ta, MIL-101–L-Pro and MIL-101–1*S*-(+)-Cam, respectively. Meanwhile, the pore volumes of the MOFs decrease from 1.363 $cm^3\ g^{-1}$ for MIL-101(Al)–NH_2 to 0.904, 0.668, 0.905, 1.085 and 1.009 $cm^3\ g^{-1}$ for MIL-101–*S*-2-Ppa, MIL-101–*R*-Epo, MIL-101–(+)-Ac-L-Ta, MIL-101–L-Pro and MIL-101–1*S*-(+)-Cam, respectively.

The SEM images indicate that the MIL-101(Al)–Xs (Fig. 3d–h) show no significant morphology change compared to MIL-101(Al)–NH_2 (Fig. 3c). The SEM images of the cross section of the bare capillary column and MIL-101(Al)–Xs-coated capillary columns show the successful coating of MIL-101(Al)–Xs onto the inner wall of the capillary columns (Fig. S3, ESI†).

The separation of racemates including alcohols, amines, nitriles, esters and aldehydes on MIL-101(Al)–Xs-coated capillary columns was carried out to evaluate their chiral separation abilities (Table S1, ESI†). 12 racemates were separated on MIL-101(Al)–Xs-coated capillary columns (Fig. 4), showing the feasibility of the PSM strategy to construct chiral MOFs for chiral GC.

The chiral selectivity of these chiral MIL-101(Al)–Xs is quite different from each other. The difference in chiral selectivity can be ascribed to different chiral recognition centers and interactions between chiral MIL-101(Al)–Xs and enantiomers.

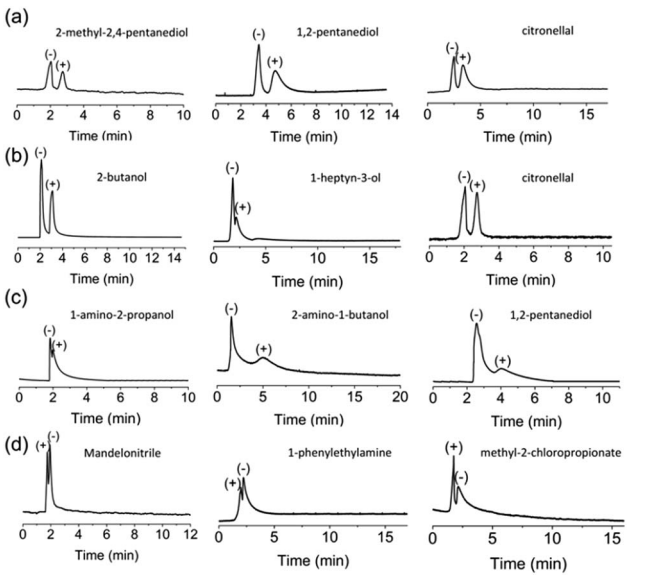

Fig. 4 GC chromatograms on the MIL-101(Al)-Xs-coated columns (30 m length × 0.25 mm i.d.) for the separation of racemates: (a) MIL-101–*S*-2-Ppa-coated column A: 2-methyl-2,4-pentanediol (160 °C, 2 ml min^{-1} N_2), 1,2-pentanediol (160 °C, 2 ml min^{-1} N_2), and citronellal (165 °C, 2 ml min^{-1} N_2). (b) MIL-101–*R*-Epo-coated column B: 2-butanol (150 °C, 2 ml min^{-1} N_2), 1-heptyn-3-ol (200 °C, 2 ml min^{-1} N_2), and citronellal (180 °C, 2 ml min^{-1} N_2). (c) MIL-101–(+)-Ac-L-Ta-coated column C: 1-amino-2-propanol (210 °C, 2 ml min^{-1} N_2), 2-amino-1-butanol (210 °C, 2 ml min^{-1} N_2), and 1,2-pentanediol (210 °C, 3 ml min^{-1} N_2). (d) MIL-101–L-Pro-coated column D: mandelonitrile (200 °C, 1.8 ml min^{-1} N_2), 1-phenylethylamine (180 °C, 2 ml min^{-1} N_2), and methyl-2-chloropropionate (180 °C, 2 ml min^{-1} N_2).

MIL-101–*S*-2-Ppa gave good resolution for olefin aldehyde and linear diols. The racemates of 2-methyl-2,4-pentanediol, 1,2-pentanediol and citronellal were baseline separated on the MIL-101–*S*-2-Ppa-coated column (Fig. 4a). The number of hydroxy groups plays key roles in chiral separation. For example, the racemates of 2-butanol, 2-pentanol and 2-hexanol with only one hydroxy group were not separated on the MIL-101–*S*-2-Ppa-coated capillary column. Moreover, such poor resolution was also observed for the separation of 1,2,6-hexanetriol racemates with three hydroxy groups. These phenomena can be ascribed to the chiral matching of diols in the chiral microenvironment and the O···H···O=C hydrogen-bonding interactions between diols and MIL-101–*S*-2-Ppa. The MIL-101–*S*-2-Ppa-coated column also gave good reproducibility for GC separation of citronellal with the relative standard deviations (RSDs) of 0.2%, 5.1% and 4.4% for the retention time, peak height and peak area, respectively. The RSDs of day-to-day and column-to-column for the separation of citronellal on the MIL-101–*S*-2-Ppa-coated column were 2.0–2.6% and 5.0–7.1%, respectively (Fig. S5; Tables S2 and S3, ESI†).

Baseline separation of citronellal racemates was achieved on the MIL-101–*R*-Epo-coated capillary column with the phenyl group, revealing the key roles of π–π interaction in chiral separation of citronellal. The MIL-101–*R*-Epo-coated capillary column gave good resolution for the racemates of 2-butanol and 1-heptyn-3-ol (Fig. 4b and S4, ESI†). MIL-101–(+)-Ac-L-Ta with only hydrogen-bonding sites in the frameworks shows poor resolution for the racemates of citronellal, but good resolution for the racemates of 1-amino-2-propanol, 2-amino-1-butanol and 1,2-pentanediol, revealing that the hydrogen-bonding interaction dominates the chiral selectivity of MIL-101–(+)-Ac-L-Ta (Fig. 4c). The hydrogen-bonding interaction caused by chiral amino acid shows a quite different selectivity for MIL-101–(+)-Ac-L-Ta. The tailing peaks of the studied racemates on the MIL-101–(+)-Ac-L-Ta-coated capillary column (Fig. 4c) can be ascribed to the strong hydrogen-bonding interactions between MIL-101–(+)-Ac-L-Ta and the racemates. All racemates separated on the MIL-101–(+)-Ac-L-Ta-coated capillary column possess two kinds of hydrogen-bonding sites ($-NH_2$ and/or –OH groups), facilitating strong hydrogen-bonding interactions between MIL-101–(+)-Ac-L-Ta and the racemates and further leading to the tailing peaks of these racemates. The racemates of mandelonitrile, 1-phenylethylamine and methyl-2-chloropropionate were separated on the MIL-101–L-Pro-coated capillary column (Fig. 4d). The separation of these racemates on the MIL-101–L-Pro-coated capillary column is not good, and it may be affected by the large BOC protecting groups, which may be stuck in the pores of MIL-101–L-Pro and lead to poor separation. However, no racemates were separated on the MIL-101–1*S*-(+)-Cam-coated capillary column. This can be ascribed to the lack of π–π and hydrogen-bonding interaction sites on 1*S*-(+)-Cam, which are quite important for chiral separation of the studied racemates. In addition, the extremely low modification percentage (4.7%) of 1*S*-(+)-Cam may also play significant roles in poor chiral separation.

Although the chiral separation mechanism is difficult to illustrate, the influence of the chiral microenvironment is essential. The kinetic diameters of all the studied racemates are smaller than the pore size of MIL-101(Al)–Xs (approximately 14 Å) (Fig. S6 and S7, ESI†), so we can assume that the chiral separation mainly occurred in the pores of the MOFs. The different chiral microenvironments constructed from various chiral centers dominate the chiral selectivity. To further confirm the importance of the chiral microenvironment of the MOFs, a (+)-diacetyl-L-tartaric anhydride-coated column was prepared for comparison. No racemates were separated on the (+)-diacetyl-L-tartaric anhydride-coated column, indicating that the synergetic effect of the chiral group and the MOF structures ensure the chiral microenvironment for chiral separation. Other interactions such as hydrogen-bonding and π–π interactions provided by chiral MIL-101(Al)–Xs also play significant roles in chiral separation.

McReynolds constants were used to evaluate the polarity of the stationary phases MIL-101(Al)-Xs (Table 1). The average McReynolds constants of MIL-101(Al)-Xs stationary phases ranged from 83 to 485, revealing weak to moderate polarities of the MIL-101(Al)–Xs-coated capillary columns. The large X values of MIL-101–*S*-2-Ppa and MIL-101–*R*-Epo resulted from their π–π stacking interaction with benzene. The large Y values of MIL-101–*S*-2-Ppa, MIL-101–*R*-Epo and MIL-101–(+)-Ac-L-Ta show their strong hydrogen-bonding ability, which gave good chiral separation for chiral alcohols and amides.

To further understand the retention and chiral discrimination of enantiomers, the enthalpy change (ΔH) and entropy change (ΔS) and the chiral part of enthalpy change ($\Delta\Delta H$) and entropy change ($\Delta\Delta S$) of the MIL-101–*S*-2-Ppa-coated column for citronellal racemates were measured (Fig. S8, ESI†). All of the determined thermodynamic parameter values are negative for the citronellal racemates (Table S4, ESI†), indicating that both the retention and chiral discrimination of the enantiomers on MIL-101–*S*-2-Ppa-coated column were driven by enthalpy.[4] Moreover, (+)-citronellal has a much larger negative ΔS than (−)-citronellal, indicating that (+)-citronellal becomes more ordered in the microenvironment of MIL-101–*S*-2-Ppa. Meanwhile, such a configuration fit is more favorable for (+)-citronellal to interact with the chiral MOFs than (−)-citronellal, resulting in a more negative value of ΔH for (+)-citronellal.

Table 1 McReynolds constants of MIL-101(Al)-Xs-coated capillary columns

Column	X[a]	Y[b]	Z[c]	U[d]	S[e]	Ave
MIL-101–*S*-2-Ppa	242	364	300	165	357	286
MIL-101–*R*-Epo	421	538	396	207	395	391
MIL-101–(+)-Ac-L-Ta	122	409	272	107	315	245
MIL-101–L-Pro	34	149	127	108	63	83
MIL-101–1*S*-(+)-Cam	−134	34	10	—	—	—

[a] X represents benzene, related to weak dispersion forces and polarizability of the phase. [b] Y refers to *n*-butanol, related to the hydrogen-bonding ability of the phase. [c] Z refers to 2-pentanone, related to the polarizability and part of the dipolar character of the phase. [d] U represents nitropropane, related to the electron donor, electron acceptor, and dipolar character of the phase. [e] S refers to pyridine, indicating the acidic character of the phase.

Two typical commercial chiral capillary columns (β-DEX 225 and CycloSil B) were employed to compare with the prepared chiral columns (Fig. S9 and S10, ESI†). The MIL-101–*S*-2-Ppa column gave much better resolution for the racemates of 2-methyl-2,4-pentanediol, 1,2-pentanediol and citronellal than the β-DEX 225 and CycloSil B columns as these analytes cannot be baseline separated on both β-DEX 225 and CycloSil B columns (Fig. S9a–c and S10a–c, and Table S1, ESI†). The MIL-101–*R*-Epo and MIL-101–(+)-Ac-L-Ta columns also gave better separation than β-DEX 225 and CycloSil B for the studied analytes. The MIL-101–L-Pro column shows comparable separation for methyl-2-chloropropionate racemates to the CycloSil B column (Fig. S10j and Table S1, ESI†), but lower resolution for 1-phenylethylamine racemates than the CycloSil B column (Fig. S10i and Table S1, ESI†). In addition, the MIL-101–L-Pro column shows better resolution for the racemates of mandelonitrile, 1-phenylethylamine and methyl-2-chloropropionate than the β-DEX 225 column (Fig. S9h–j and Table S1, ESI†). These results reveal the great potential of PSM to synthesize chiral MOFs for chiral separation.

Conclusions

In summary, we have reported a convenient PSM approach to design and synthesize chiral MOFs with different chiral sites for chiral separation. Five different post-modified chiral groups were chosen to elucidate and tune the chiral selectivity of these chiral MOFs. The resolution of the studied racemates on chiral MOF capillary columns is superior to that of the commercial β-DEX 225 and Cyclosil B chiral capillary columns. The chiral selectivity of these MOFs is quite different due to their different post-modified chiral groups. The chiral environment, and π–π and hydrogen-bonding interactions of the chiral MOFs play key roles in chiral GC. Thus, we can apply the specific interaction between the post-modified group and racemate for the rational design of diverse target chiral MOFs for chiral separation, which can avoid the blind synthesis of chiral MOFs. This work also provides a new way to design and synthesize novel CSPs for chiral chromatography.

Conflicts of interest

The authors declare no conflict of interest.

Acknowledgements

This work was supported by the National Natural Science Foundation of China (No. 21775056 and 21777074), the National Basic Research Program of China (No. 2015CB932001), the National First-class Discipline Program of Food Science and Technology (No. JUFSTR20180301), and the Fundamental Research Funds for the Central Universities (No. JUSRP11844 and JUSRP51714B).

References

1 Y. Liu, W.-M. Xuan and Y. Cui, *Adv. Mater.*, 2010, **22**, 4112–4135.
2 M. Zhang, X.-L. Chen, J.-H. Zhang, J. Kong and L.-M. Yuan, *Chirality*, 2016, **28**, 340–346.
3 H.-L. Qian, C.-X. Yang and X.-P. Yan, *Nat. Commun.*, 2016, **7**, 12104.
4 C.-H. Deng, T. Li, J.-H. Chen, J.-G. Ma and P. Cheng, *Dalton Trans.*, 2017, **46**, 6830–6834.
5 J.-H. Zhang, S.-M. Xie, B.-J. Wang, P.-G. He and L.-M. Yuan, *J. Chromatogr. A*, 2015, **1426**, 174–182.
6 X. Han, J.-J. Huang, C. Yuan, Y. Liu and Y. Cui, *J. Am. Chem. Soc.*, 2018, **140**, 892–895.
7 J.-Q. Dong, Y. Liu and Y. Cui, *Chem. Commun.*, 2014, **50**, 14949–14952.
8 Z.-Y. Gu and X.-P. Yan, *Angew. Chem., Int. Ed.*, 2010, **49**, 1477–1480.
9 N. Chang, Z.-Y. Gu and X.-P. Yan, *J. Am. Chem. Soc.*, 2010, **132**, 13645–13647.
10 M. M. Wanderley, C. Wang, C.-D. Wu and W.-B. Lin, *J. Am. Chem. Soc.*, 2012, **134**, 9050–9053.
11 C.-F. Zhu, G.-Y. Yuan, X. Chen, Z.-W. Yang and Y. Cui, *J. Am. Chem. Soc.*, 2012, **134**, 8058–8061.
12 M. C. Das, Q.-S. Guo, Y.-B. He, J. Kim, C.-G. Zhao, K.-L. Hong, S.-C. Xiang, Z.-J. Zhang, K. M. Thomas, R. Krishna and B.-L. Chen, *J. Am. Chem. Soc.*, 2012, **134**, 8703–8710.
13 P. Li, Y.-B. He, J. Guang, L.-H. Weng, J. C.-G. Zhao, S.-C. Xiang and B.-L. Chen, *J. Am. Chem. Soc.*, 2014, **136**, 547–569.
14 S.-M. Xie, Z.-J. Zhang, Z.-Y. Wang and L.-M. Yuan, *J. Am. Chem. Soc.*, 2011, **133**, 11892–11895.
15 X. Kuang, Y. Ma, H. Su, J. Zhang, Y.-B. Dong and B. Tang, *Anal. Chem.*, 2014, **86**, 1277–1281.
16 M. Zhang, Z.-J. Pu, X.-L. Chen, X.-L. Gong, A.-X. Zhu and L.-M. Yuan, *Chem. Commun.*, 2013, **49**, 5201–5203.
17 Y.-W. Peng, T.-F. Gong, K. Zhang, X.-C. Lin, Y. Liu, J.-W. Jiang and Y. Cui, *Nat. Commun.*, 2014, **2**, 5406.
18 M. Banerjee, S. Das, M. Yoon, H. J. Choi, M. H. Hyun, S. M. Park, G. Seo and K. Kim, *J. Am. Chem. Soc.*, 2009, **131**, 7524–7525.
19 X. Wang, W.-X. Chen, L. Zhang, T. Yao, W. Liu, Y. Lin, H.-X. Ju, J.-C. Dong, L.-R. Zheng and W.-S. Yan, *J. Am. Chem. Soc.*, 2017, **139**, 9419–9422.
20 S. Bernt, V. Guillerm, C. Serre and N. Stock, *Chem. Commun.*, 2011, **47**, 2838–2840.
21 J.-Q. Jiang, C.-X. Yang and X.-P. Yan, *Chem. Commun.*, 2015, **51**, 6540–6543.
22 S. J. Garibay, Z.-Q. Wang, K. K. Tanabe and S. M. Cohen, *Inorg. Chem.*, 2009, **48**, 7341–7349.
23 K. K. Tanabe and S. M. Cohen, *Angew. Chem., Int. Ed.*, 2009, **48**, 7424–7427.
24 Y.-R. Du, X.-Q. Li, X.-J. Lv and Q. Jia, *ACS Appl. Mater. Interfaces*, 2017, **9**, 30925–30932.
25 H.-T. Zhu, L.-N. Wang, X.-M. Jie, D.-D. Liu and Y.-M. Cao, *ACS Appl. Mater. Interfaces*, 2016, **8**, 22696–22704.
26 P. Serra-Crespo, E. V. Ramos-Fernandez, J. Gascon and F. Kapteijn, *Chem. Mater.*, 2011, **23**, 2565–2572.
27 J. Bonnefoy, A. Legrand, E. A. Quadrelli, J. Canivet and D. Farrusseng, *J. Am. Chem. Soc.*, 2015, **137**, 9409–9416.

28 E. Dugan, Z.-Q. Wang, M. Okamura, A. Medina and S. M. Cohen, *Chem. Commun.*, 2008, **29**, 3366–3368.
29 S. J. Garibay, Z.-Q. Wang and S. M. Cohen, *Inorg. Chem.*, 2010, **49**, 8086–8091.
30 K. K. Tanabe, Z.-Q. Wang and S. M. Cohen, *J. Am. Chem. Soc.*, 2008, **130**, 8508–8517.
31 T. Liu, J.-X. Che, Y.-Z. Hu, X.-W. Dong, X.-Y. Liu and C.-M. Che, *Chem.–Eur. J.*, 2014, **20**, 14090–14095.
32 J. Navarro-Sanchez, A. I. Argente-Garcia, Y. Moliner-Martinez, D. Roca-Sanjuan, D. Antypov, P. Campins-Falco and M. J. Rosseinsky, *J. Am. Chem. Soc.*, 2017, **139**, 4294–4297.